

Tidal Disruption of Strengthless Rubble Piles— A Dimensional Analysis

Joseph M. Hahn
Lunar and Planetary Institute
3600 Bay Area Boulevard
Houston, TX 77058-1113
hahn@lpis58.jsc.nasa.gov

Terrence W. Rettig
Department of Physics
University of Notre Dame
Notre Dame, IN 46556
Terrence.W.Rettig.1@nd.edu

To appear in *Planetary and Space Science*

ABSTRACT

A relatively simple prescription for estimating the number of debris clumps n that form after a catastrophic tidal disruption event is presented. Following the breakup event, it is assumed that the individual debris particles follow keplerian orbits about the planet until the debris’ gravitational contraction timescale t_c becomes shorter than its orbital spreading timescale t_s . When the two timescales become comparable, self-gravity breaks up the debris train into $n \sim L/D$ clumps, which is the debris length/diameter ratio at that instant. The clumps subsequently orbit the planet independent of each other. The predicted number of clumps n is in good agreement with more sophisticated N -body treatments of tidal breakup for parabolic encounters, and the dependence of n upon the progenitor’s density as well as its orbit is also mapped out for hyperbolic encounters. These findings may be used to further constrain both the orbits and densities of the tidally disrupted bodies that struck Callisto and Ganymede. A cursory analysis shows that the Gomul and Gipul crater chains on Callisto, which have the greatest number of craters among the known chains, were formed by projectiles having comet-like densities estimated at $\rho_0 \lesssim 1$ gm/cm³.

1. Introduction

The brief and dramatic appearance of Comet Shoemaker–Levy 9 (S–L 9) has contributed to the notion that many small members of the solar system might be strengthless ‘rubble-piles’, that is, material conglomerates having no significant structural strength other than their self-gravity (e.g., Davis *et al.* 1979, Weissman 1986). As models of the S–L 9 encounter with Jupiter indicate, only a relatively strengthless rubble-pile is able to catastrophically disrupt into a cloud of debris that later condenses into twenty or so gravitating clumps having the S–L 9 ‘string-of-pearls’ morphology (Asphaug and Benz 1994, 1996; Solem 1994). Further, it appears that similar events have occurred repeatedly in the Jovian system, as evidenced by the crater chains that scar two of the Galilean satellites with linear arrangements similar to the S–L 9 fragment chain (Melosh and Schenk 1993, McKinnon and Schenk 1995, and Schenk *et al.* 1996).

N -body simulations of tidal breakup have been used to extract size and density estimates of the S–L 9 progenitor with great precision (Asphaug and Benz 1994, 1996; Solem 1994), and similar models are used to investigate the tidal disruption of asteroids by Earth (Bottke *et al.* 1997a,b). An order-of-magnitude discussion of tidal breakup is also given in Rettig *et al.* (1996). Below, the tidal disruption phenomenon is examined in a heuristic fashion by comparing the relevant timescales: the debris spreading timescale t_s over which differential orbital motions cause the debris to spread, versus the contraction timescale t_c over which the debris self-gravity causes it to condense into a few clumps. This comparison will demonstrate how the number of debris clumps formed depends upon the projectile’s physical properties as well as its orbit. The intent of this analysis is not only to complement the extant numerical studies of tidal disruption, but also to extend them to as-yet unexplored regions of parameter space.

2. Breakup mechanics

In order to illustrate the phenomenon of gravitational recondensation of tidally disrupted debris, consider the relevant timescales governing the debris’ evolution. After a projectile is tidally disrupted, all of its debris particles are injected into distinct orbits that cause them to drift apart largely along a single axis. By tracking their motions, the spreading timescale t_s over which the debris train grows in length is easily computed. Concurrently, debris self-gravity endeavors to contract this material, and this proceeds over a timescale t_c . So long as $t_s \ll t_c$, the debris continues to spread relatively unimpeded by its own gravity. But if t_c should ever become smaller than t_s , then the local gravity will dominate the motions of the individual particles and the debris train will break up

into distinct gravitationally bound clumps of material. Of course the clumps themselves continue to drift apart due to their differing orbits. This was evidently the fate of Comet Shoemaker–Levy 9 as well as the impactors responsible for the crater chains on the Galilean satellites.

N -body simulations of this phenomenon have already shown that the resulting number of clumps depends sensitively on the projectile’s initial density ρ_0 and its periaipse distance r_0 . Since the orbit of Comet S–L 9 was known, Asphaug and Benz (1994) and Solem (1994) were able infer its density with a high degree of precision. The primary virtue of the following analysis is that it reveals *how* the number of clumps scales with ρ_0 and r_0 . And, as an application of the theory, the crater chains seen on the Galilean satellites are considered, from which upper limits on the projectiles’ densities are estimated. Tidal disruption of parabolic projectiles is addressed first, as this is the appropriate encounter scenario for bodies like S–L 9 that are first captured by a planet from a heliocentric orbit. The analysis is then repeated for hyperbolic encounters.

2.1. Parabolic encounters

The timescale t_s over which the tidally disrupted debris grows in length is easily estimated from simple two–body mechanics. It is assumed here that the incoming projectile is on a parabolic orbit and is a non-rotating spherical body of radius R that remains intact and undeformed until periaipse passage. It is also assumed that the projectile breaks up into numerous particles at this moment, and that each particle subsequently follows individual keplerian orbits about the planet. At the moment of breakup, each debris particle has a velocity $V_0 = \sqrt{2GM/r_0}$ perpendicular to the direction of the planet of mass M which lies a distance r_0 away from the projectile’s center, and G is the gravitation constant. The surface particle nearest the planet has a specific energy $E = -GM/2a_1 = V_0^2/2 - GM/(r_0 - R)$ and periaipse distance $r_0 - R = a_1(1 - e_1)$, which yield its semi–major axis a_1 and eccentricity e_1 :

$$a_1 = \frac{1 - \beta}{2\beta} r_0 \quad \text{and} \quad e_1 = 1 - 2\beta, \tag{1}$$

where $\beta \equiv R/r_0$ is the dimensionless radius of the projectile. This particle enters an elliptic orbit about the planet and remains at one end of the debris train. Similarly, the surface particle furthest from Jupiter lies at the other end of the debris train and follows a hyperbolic orbit with elements given by Eqn. (1) but with an opposite sign on β .

The trajectory of a debris particle formerly at the projectile’s center is $\mathbf{r}(t)$, which is

governed by the parabolic orbit equation and Kepler’s equation:

$$\frac{r}{r_0} = 1 + \tan^2(\theta/2) \quad \text{and} \quad \frac{t}{\tau} = \sqrt{2}[\tan(\theta/2) + \frac{1}{3}\tan^3(\theta/2)], \quad (2)$$

where t is the time since periape passage, $\tau \equiv \sqrt{r_0^3/GM}$ is the encounter timescale, and θ is this particle’s true anomaly. The surface particle in the interior orbit has an elliptic trajectory $\mathbf{r}_1(t)$ given by

$$r_1 = a_1(1 - e_1 \cos E) \quad \text{and} \quad \frac{t}{\tau} = \left(\frac{a_1}{r_0}\right)^{3/2} (E - e_1 \sin E), \quad (3)$$

where E is the particle’s eccentric anomaly, and its true anomaly θ obeys $\sqrt{1 - e_1} \tan \theta/2 = \sqrt{1 + e_1} \tan E/2$.

The debris length in units of the projectile’s diameter $D = 2\beta r_0$ is $L/D = |\mathbf{r} - \mathbf{r}_1|/\beta r_0$, which is easily computed numerically using Eqns. (2-3) and is displayed in Fig. 1. It has been verified that this curve is indeed independent of β when $\beta \ll 1$. This computation is essentially that of Scotti and Melosh 1993, who also neglect debris gravity but do include perturbations by the Sun and other planets, and yielded the first size estimate of the S–L 9 progenitor based on comparisons to early observations of the Comet. Figure 1 also includes results from an N -body simulation of the S–L 9 encounter with Jupiter, which shows that the simple prescription employed here is sufficiently accurate (for these purposes) for estimating the length of the tidally disrupted debris over time. The good agreement between the two approaches is also noted by Asphaug and Benz (1996).

From Fig. 1, the debris spreading timescale $t_s \equiv L/(dL/dt)$ is computed numerically and plotted against the debris length L/D in Fig. 2. As one might expect of debris in highly eccentric orbits, their spreading timescale increases as their orbital motions slow with distance from the planet.

2.2. Gravitational contraction

Since t_s grows over time, it is possible that the debris spreading due to its orbital evolution becomes so slow that its local gravity can cause it to clump up, creating a morphology similar to the S–L 9 ‘string of pearls’. The timescale for gravitational contraction will vary as the free-fall timescale $t_c = \alpha/\sqrt{G\rho}$, where ρ is the debris density. If the debris were a stationary cloud of collisionless particles, then the free-fall time has $\alpha = \sqrt{3\pi/32} \simeq 0.54$ (Binney and Tremaine 1987). However tidally disrupted debris is neither, so a larger value for α is anticipated due to the particles’ motions.

Inspection of the N -body simulations shows that the debris spreads largely along a single axis (Asphaug and Benz 1994, 1996), hence, its density varies as $\rho \sim \rho_0 D/L$ where ρ_0 is the projectile’s initial density. The gravitational contraction timescale is then

$$\frac{t_c}{\tau} \sim \alpha \sqrt{\frac{\rho_c L}{\rho_0 D}} \quad (4)$$

where $\rho_c \equiv M/r_0^3$ is the critical density. The critical density is termed thus since an inviscid body on a parabolic orbit will suffer tidal disruption only if its density obeys $\rho_0 \lesssim 1.16\rho_c$ (Sridhar and Tremaine 1992). Figure 2 plots t_c/τ against L/D for various values of ρ_0/ρ_c and assuming $\alpha \simeq 1$; this choice of α is justified below.

So long as $t_s < t_c$, the debris elongates due to their orbital motions. But once $t_c < t_s$, local gravity will contract the debris at a rate faster than it is spread by its orbital motions. In this regime, gravitational contraction of each forming clump will proceed homologously across the debris’ shortest spatial scale, its diameter D . This produces $n \sim L/D$ gravitationally bound clumps condensing from the debris, where L is the debris length at the moment when $t_c \sim t_s$. This quantity may be obtained directly from the ordinate of Fig. 2 where the timescales t_c and t_s cross for a given value of ρ_0/ρ_c .

In order to calibrate the unknown parameter α , results from the Asphaug and Benz (1994) N -body simulation of the S–L 9 breakup is used as a standard. To obtain $n = 20$ fragments from a projectile of density $\rho_0 = 0.5 \text{ gm/cm}^3$ encountering a planet of mass $M = 1.9 \times 10^{30} \text{ gm}$ at a periape distance of $r_0 = 9.4 \times 10^4 \text{ km}$, for which $\rho_c = 2.29 \text{ gm/cm}^3$ and $\rho_0/\rho_c = 0.22$, a value of $\alpha = 0.94$ is required (see Fig. 2). However it may only be concluded that α is of order unity as this simple treatment also ignores other effects such as the tidal elongation the projectile suffers during the moments before breakup. From Fig. 2 it is evident that the resulting number of clumps depends rather sensitively on the projectile’s density due to the fact that the t_s and t_c curves have a rather similar power-law dependence.

Figure 3 shows the estimated number of clumps $n \sim L/D$ that form as the debris train breaks up (*ie.*, when $t_c = t_s$) as a function of projectile density ρ_0/ρ_c . The data points accompanying this figure are from N -body simulations of S–L 9 type tidal disruption events (Asphaug and Benz 1994, Solem 1994). Asphaug and Benz (1994) quote only lower limits on the number of clumps produced in their simulations, perhaps because the distinction between gravitating clumps and unconsolidated material is a subjective one. Thus their results are represented by arrows in Fig. 3. Those models also indicate that at least 500 to 1000 particles are necessary to numerically resolve all the clumps produced by S–L 9’s disruption. Since fewer particles were employed in the Solem (1994) models, those results are also interpreted here as lower limits. From this comparison it may be concluded that

the very general (and simple) timescale analysis employed here agrees qualitatively with the far more CPU-intensive N -body simulations that are available in the literature.

2.3. Hyperbolic encounters

The preceding analysis is now extended to hyperbolic projectiles that approach close enough to a planet to tidally disrupt. The incoming projectile’s orbit elements may be written $a_0/r_0 = -(V_e/V_\infty)^2/2$ and $e_0 = 1 - r_0/a_0$, where r_0 is again the periaipse distance of the projectile’s center, $V_e = \sqrt{2GM/r_0}$ is the planet’s escape velocity at periaipse, and V_∞ is the projectile’s velocity far from the planet. As before, the spherical, non-rotating projectile is assumed to remain intact and undeformed until periaipse, after which it breaks up and its debris follows keplerian orbits. The specific energy of the surface particle nearest the planet again provides its orbit elements:

$$\frac{a_1}{r_0} = \left(\frac{r_0}{a_0} + \frac{2\beta}{1-\beta} \right)^{-1} \quad \text{and} \quad e_1 = e_0 - \beta(1 + e_0). \quad (5)$$

The trajectories \mathbf{r}_i for particles $i = 0$ (which lies at the center of the debris train) and $i = 1$ (which lies at one end of the train) are given by

$$r_i = a_1(1 - e_i \cosh E) \quad \text{and} \quad \frac{t}{\tau} = \left(-\frac{a_i}{r_0} \right)^{3/2} (e_i \sinh E - E), \quad (6)$$

where E is the eccentric anomaly and the true anomaly θ_i is obtained from $e_i \cos \theta = (1 - \beta)(1 + e_i)/(r_i/r_0) - 1$ with $\beta = 0$ for particle 0. The debris length $L/D = |\mathbf{r}_0 - \mathbf{r}_1|/\beta r_0$ is obtained numerically by solving Eqns. (6) for various values of the projectile’s dimensionless velocity $V \equiv V_\infty/V_e$ (see Fig. 4). Note that slower projectiles produce longer debris trains since the planet is more effective at scattering the debris particles through a wider spread of angles. From the curves in Fig. 4, the debris spreading timescale $t_s = L/(dL/dt)$ is computed and displayed in Fig. 5 versus L/D .

Figure 5 also shows the debris’ gravitational contraction timescale t_c/τ , Eq. (4), for various projectile densities ρ_0/ρ_c . As before, the estimated number of clumps formed when local gravity breaks up the debris train is simply the value of L/D where these timescale curves cross. The results from this procedure are summarized in Fig. 6 which shows the number of clumps formed versus projectile density ρ_0/ρ_c for selected velocities V . The $V = 0$ curve is for a parabolic projectile that also appears in Fig. 3, and has a power-law dependence distinct from the hyperbolic projectiles. This is due to the faster growth rate of parabolic debris, which varies as $L \sim t^{4/3}$ (Sridhar and Tremaine 1992), whereas the hyperbolic debris elongates linearly with time.

It is important to keep in mind that all of the curves presented here are for a spherical non-rotating projectile. For this reason Fig. 6 does not include data from the only N -body simulation of a hyperbolic encounter presently available (e.g., Bottke *et al.* 1997a), since that projectile was elongated by a factor of 1.8 and rotating at about 40% of its centrifugal limit. Nonetheless, this region of parameter space warrants further exploration. It is likely that Fig. 6 underestimates the number of clumps that would be formed after the disruption of an elongated projectile. And, as Asphaug and Benz (1994) and Solem (1994) show, prograde rotation lengthens the debris train and produces greater numbers of clumps, whereas retrograde rotation yields a shorter train with fewer clumps. Furthermore, a projectile having a rotation axis in the orbit plane will likely have a more distended debris train which will impede its subsequent contraction and increase the number of clumps formed.

3. Crater chains

The preceding results can also be applied to the crater chains seen on the Galilean satellites Ganymede and Callisto, which were likely formed by tidally disrupted bodies striking the satellites on the outbound legs of their orbits (Melosh and Schenk 1993, McKinnon and Schenk 1995, Schenk *et al.* 1996). It will be assumed here that these bodies, like S-L 9, disrupted *catastrophically* into numerous debris particles which subsequently recondensed into n clumps before impacting the satellite and creating a linear chain of n craters. Since the impactors' orbits are constrained by tidal disruption requirements, upper limits on the projectiles' densities ρ_0 are obtained directly.

Ganymede and Callisto orbit Jupiter at a distance of $r_s = 15.0$ and $26.3 R_J$, respectively, where $R_J = 7.15 \times 10^4$ km is the radius of Jupiter. If a projectile responsible for a crater chain was a long-period comet on a parabolic orbit about the Sun, it would approach the Jovian system with a velocity that is of order $V_\infty \sim \sqrt{2GM_\odot/a_J}$, where M_\odot is the mass of the Sun and a_J is Jupiter's semi-major axis. Thus its dimensionless velocity $V \equiv V_\infty/V_e$ is limited to

$$V \lesssim \sqrt{\frac{r_s}{a_J} \frac{M_\odot}{M}} \quad (7)$$

since a projectile's periape $r_0 < r_s$ must lie interior to the satellite's orbit. This limits $V \lesssim 1.2$ (1.6) for Ganymede (Callisto). However McKinnon and Schenk (1995) argue that short-period comets with velocities $V_\infty \simeq 4.5$ to 8 km/sec dominate the flux of bodies encountering Jupiter; if the latter velocity is adopted here then $V \lesssim 0.5$ (0.7) for Ganymede (Callisto).

The tightest density constraint is obtained from the Gomul crater chain on Callisto, which has $n = 25$ craters (Schenk *et al.* 1996). Examination of Fig. 6 shows that this projectile had a density $0.06 \lesssim \rho_0/\rho_c \lesssim 0.2$ for $V \lesssim 0.7$. Since the projectile’s periapse must lie outside of the planet, $r_0 > 1R_J$ and thus $\rho_0 \lesssim 1.0 \text{ gm/cm}^3$. A similar estimate is obtained for the $n = 18$ Gipul crater chain on Callisto, and the projectiles that formed the remaining crater chains reported by Schenk *et al.* (1996) may be shown to have maximal densities estimated at $\rho_o \lesssim 1.6$ to 2.4 gm/cm^3 . While this analysis does not place particularly tight limits on the densities of most of these projectiles, these findings are consistent with the Gomul and Gipul crater chains as being due to impacts by tidally disrupted cometary debris rather than due to asteroidal debris. However, placing tighter constraints on the projectiles’ densities would require extracting the projectiles’ orbits (e.g., r_0 and V_∞) from the crater record.

4. Summary and conclusions

A simple algorithm that estimates the number of clumps n that form after a catastrophic tidal disruption event is obtained. It is assumed here that a projectile approaches the planet undeformed, and that following breakup, the debris particles follow keplerian orbits until their gravitational contraction timescale t_c becomes comparable to their spreading timescale t_s . Even though these assumptions ignore the consequences of the tidal distortion and torque suffered by the incoming projectile, the resulting debris evolution (e.g., Fig. 1) is in good agreement with more sophisticated treatments. It is argued here that once the spreading and contraction timescales become comparable, the debris breaks up into $n \sim L/D$ gravitationally bound clumps having a morphology similar to S–L 9’s fragmented appearance.

This treatment compares favorably with existing N –body treatments of tidal breakup of parabolic encounters, and the analysis is extended to hyperbolic encounters. Disrupted projectiles that encounter the planet at higher velocities $V \equiv V_\infty/V_e > 0$ will be scattered into trajectories having a smaller angular spread. This results in more compact debris that breaks up into fewer numbers of clumps at distances closer to the planet (see Fig. 5). Thus if the projectiles responsible for the chains of $n \sim \mathcal{O}(10)$ craters on Ganymede and Callisto were hyperbolic (*i.e.*, $V \gtrsim 1$), then they surely had comet–like densities $\rho_0 \lesssim 0.1\rho_c \sim 0.5 \text{ gm/cm}^3$ (from Fig. 6 and noting that periapse must lie outside the planet). But if these projectiles were parabolic (*i.e.*, $V \ll 1$), then only rather soft limits (e.g., $\rho_0 \lesssim 1.0$ to 2.4 gm/cm^3) on their estimated densities are obtained.

Acknowledgements

The authors thank Bill Ward for his thoughts and assistance with this work. This paper is Contribution 947 from the Lunar and Planetary Institute, which is operated by the Universities Space Research Association under NASA Contract NAGW-4575.

REFERENCES

- Asphaug, E. and W. Benz (1994). Density of Comet Shoemaker–Levy 9 deduced by modeling breakup of the parent ‘rubble pile’. *Nature* **370**, 120–123.
- Asphaug, E. and W. Benz (1996). Size, density, and structure of Comet Shoemaker–Levy 9 inferred from the physics of tidal breakup. *Icarus* **121**, 225–248.
- Binney, J. and S. Tremaine (1987). *Galactic Dynamics*, pg. 37. Princeton University Press, Princeton, NJ.
- Bottke, W. F., D. C. Richardson, and S. G. Love (1997). Can tidal disruption of asteroids make crater chains on Earth and Moon *Icarus* **126**, 470–474.
- Bottke, W. F., D. C. Richardson, and S. G. Love, (1997). Production of Tunguska–sized bodies by Earth’s tidal forces. *Planetary and Space Science*, in press.
- Davis, D. R., C. R. Chapman, R. Greenberg, and S. J. Weidenschilling (1979). Collisional evolution of asteroids: populations, rotations, and velocities. In *Asteroids* (T. Gehrels, Ed.), pg. 528–557. Univ. of Arizona Press, Tuscon.
- Melosh, H. J. and P. Schenk (1993). Split comets and the origin of crater chains on Ganymede and Callisto. *Nature* **365**, 731–733.
- McKinnon, and Schenk, (1995). Estimates of comet fragment masses from impact crater chains on Callisto and Ganymede. *GRL* **22**, 1829–1832.
- Rettig, T. W., M. J. Mumma, G. J. Sobczak, J. M. Hahn, and M. DiSanti (1996). The nature of comet Shoemaker–Levy 9 subnuclei from analysis of preimpact Hubble Space Telescope images. *JGR* **101**, 9271–9281.
- Scotti, J. V., and H. J. Melosh (1993). Estimate of the size of comet Shoemaker–Levy 9 from a tidal breakup model. *Nature* **365**, 733–735.
- Schenk, P. M., E. Asphaug, W. B. McKinnon, H. J. Melosh, and P. R. Weissman (1996). Cometary nuclei and tidal disruption: the geologic record of crater chains on Callisto and Ganymede. *Icarus* **121** 249–274.
- Solem, J. C. (1994). Density and Size of Comet Shoemaker–Levy 9 deduced from a tidal breakup model. *Nature* **370**, 349–351.
- Sridhar, S. and S. and Tremaine (1992). Tidal disruption of viscous bodies. *Icarus* **95**, 86–99.

Weissman, P. R. (1986). Are cometary nuclei primordial rubble piles? *Nature* **320**, 242–244.

FIGURE CAPTIONS

Fig. 1.— The length of the debris train L/D plotted against time t/τ (thick curve) and against radial distance r/r_0 from the planet (thin curve). The data points are L/D from the Asphaug and Benz (1996) N -body simulation of the S–L 9 encounter, plotted versus time (\bullet) and distance (open box). The discrepancy evident just after breakup is due to the fact that this analysis does not account for the tidal elongation experienced by the model projectile as it approached periapse.

Fig. 2.— The debris spreading timescale t_s/τ versus debris length L/D (thick curve). Time and distance from the planet advance to the right. Note that t_s is initially large due to the debris’ slow growth when $L/D \lesssim 1.5$ (see Fig. 1). Also plotted is the gravitational contraction timescale t_c/τ versus L/D for selected projectile densities $\rho \equiv \rho_0/\rho_c$. Gravitational contraction is impossible while the debris still lies within the planet’s modified Roche limit $r/r_0 < 1.05(\rho_c/\rho_0)^{1/3}$ (Sridhar and Tremaine (1992)), which is indicated by the dotted curves. The estimated number of clumps n is simply the value of L/D where the two timescales cross. To calibrate this analysis with the N -body models of the S–L 9 breakup requires $\alpha = 0.94$, which yields $n \sim L/D = 20$ clumps where the t_s/τ timescale crosses the t_c/τ curve for $\rho = 0.22$, which is indicated by the dot.

Fig. 3.— The estimated number of clumps n versus projectile density ρ_0/ρ_c . The data points are from the Asphaug and Benz (1994) (\bullet) and Solem (1994) (+) models of the S–L 9 breakup, with the arrows indicating lower limits. The upper density axis is scaled for the S–L 9 encounter which has $\rho_c = 2.29 \text{ gm/cm}^3$.

Fig. 4.— Debris train length L/D versus time t/τ for selected values of the projectile velocity $V \equiv V_\infty/V_e$. The $V = 0$ curve is for the parabolic projectile also shown in Fig. 1.

Fig. 5.— The debris spreading timescale t_s/τ versus debris length L/D for various velocities $V \equiv V_\infty/V_e$ (thick curves). The narrow curves give the debris contraction timescale t_c/τ versus L/D for various projectile densities $\rho \equiv \rho_0/\rho_c$ and $\alpha = 0.94$. The value of L/D where these curves cross is the estimated number of clumps formed when the debris train breaks up.

Fig. 6.— The estimated number of clumps n versus projectile density ρ_0/ρ_c for various projectile velocities $V \equiv V_\infty/V_e$. The $V = 0$ curve is for the parabolic projectile given in Fig. 3. The upper density axis is scaled for an encounter at Earth having an arbitrary perigee distance $r_0 = 1.5$ Earth–radii for which $\rho_c = 2.29 \text{ gm/cm}^3$.

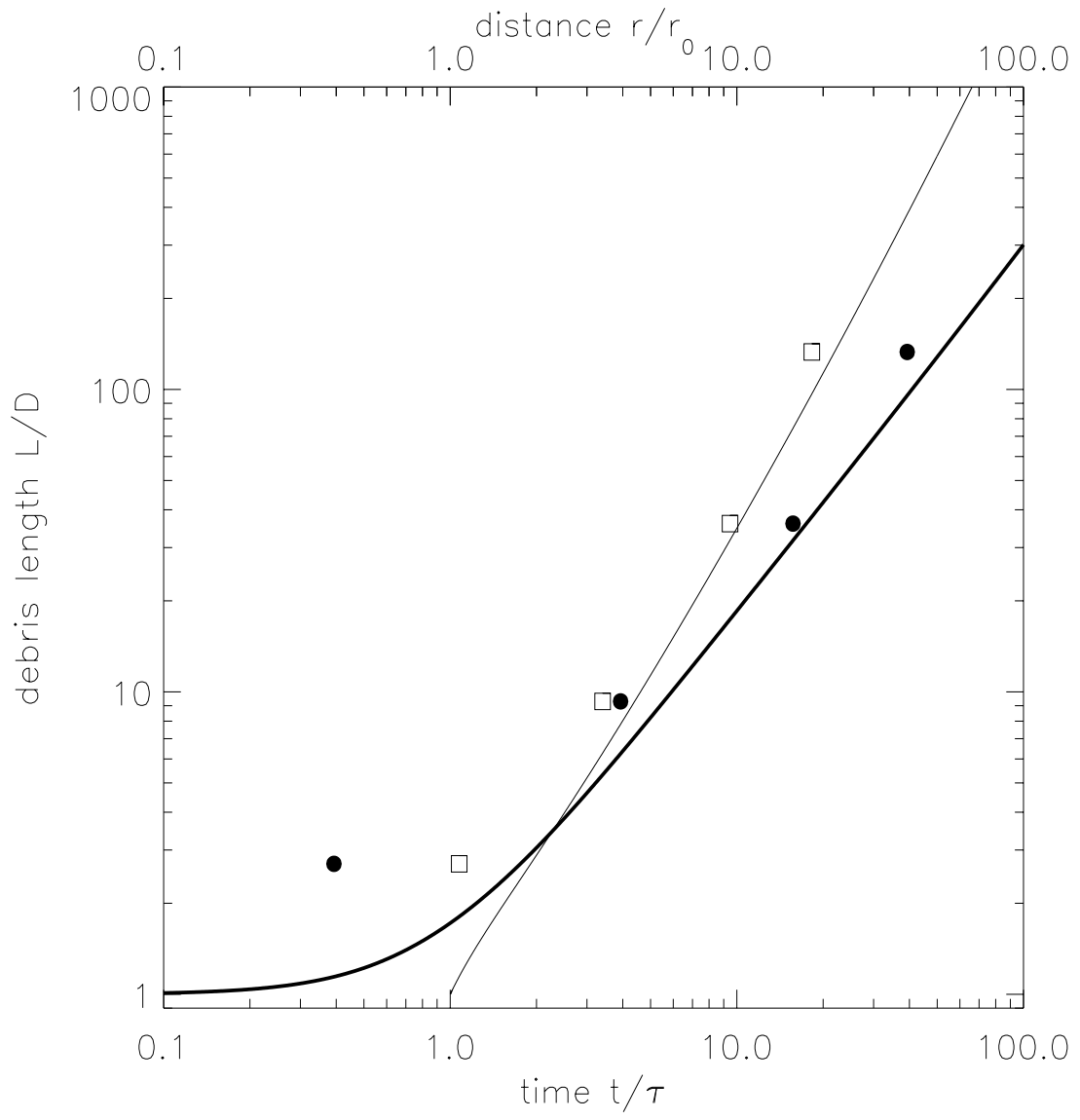


Fig. 1.

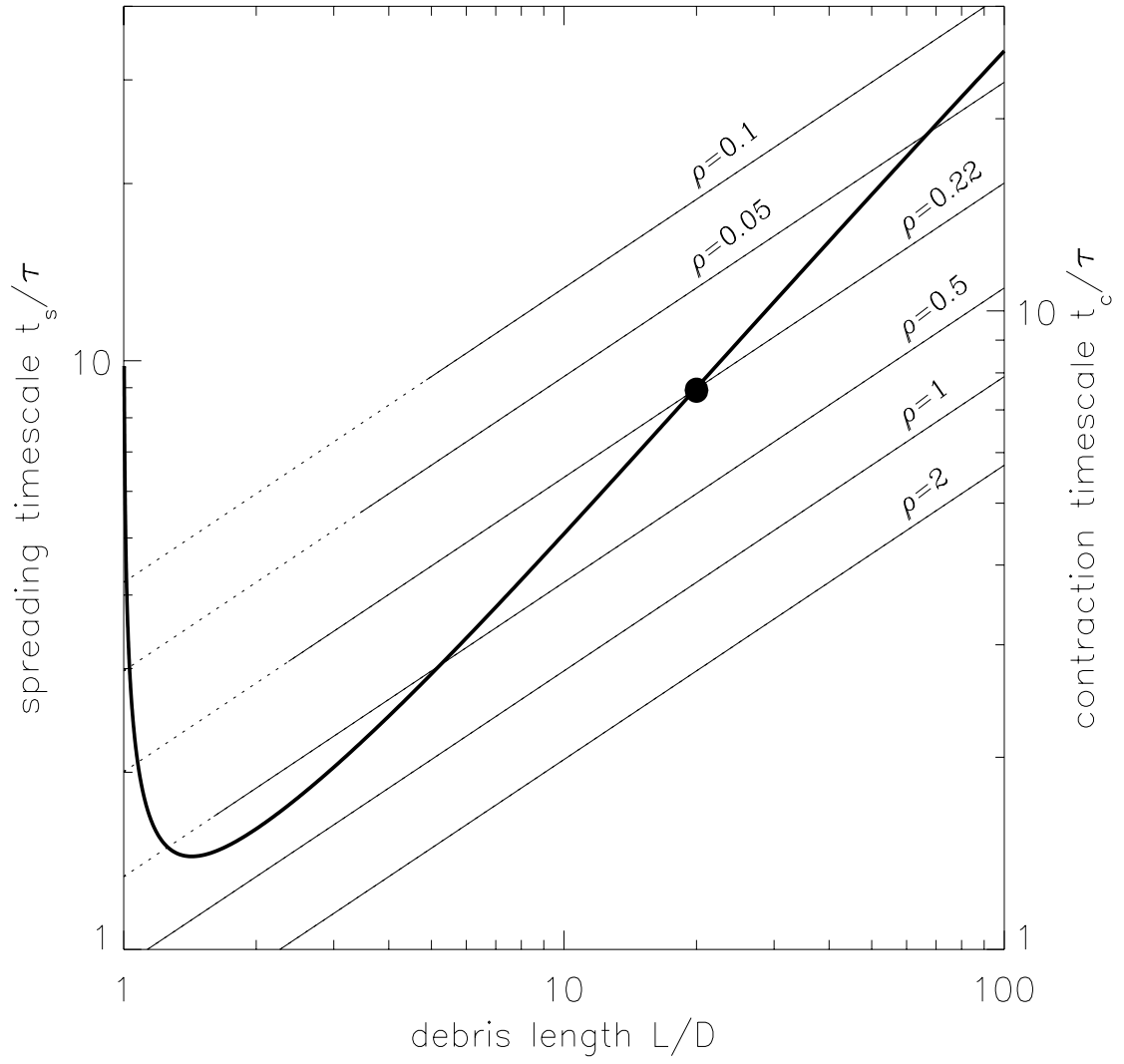


Fig. 2.

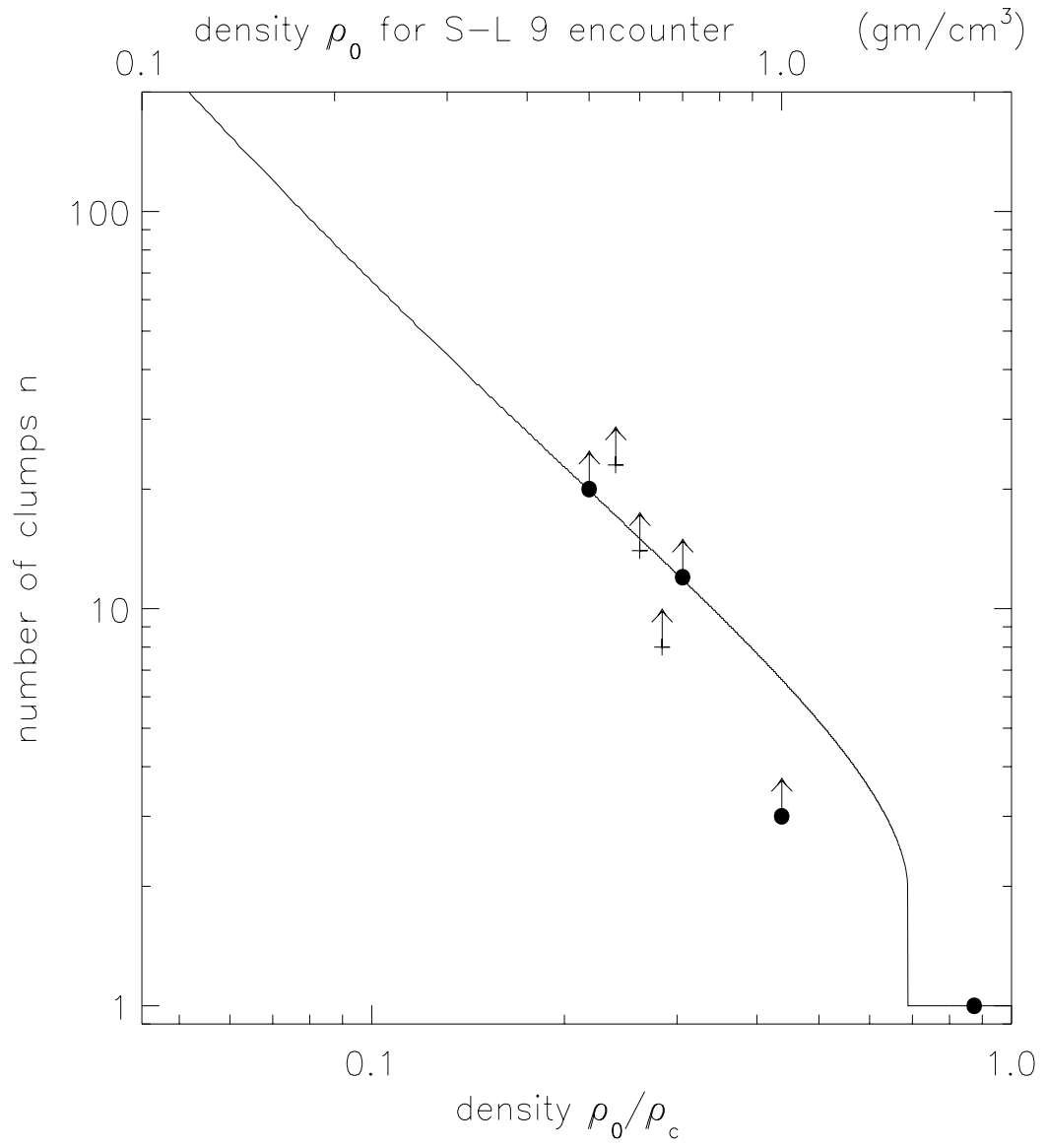


Fig. 3.

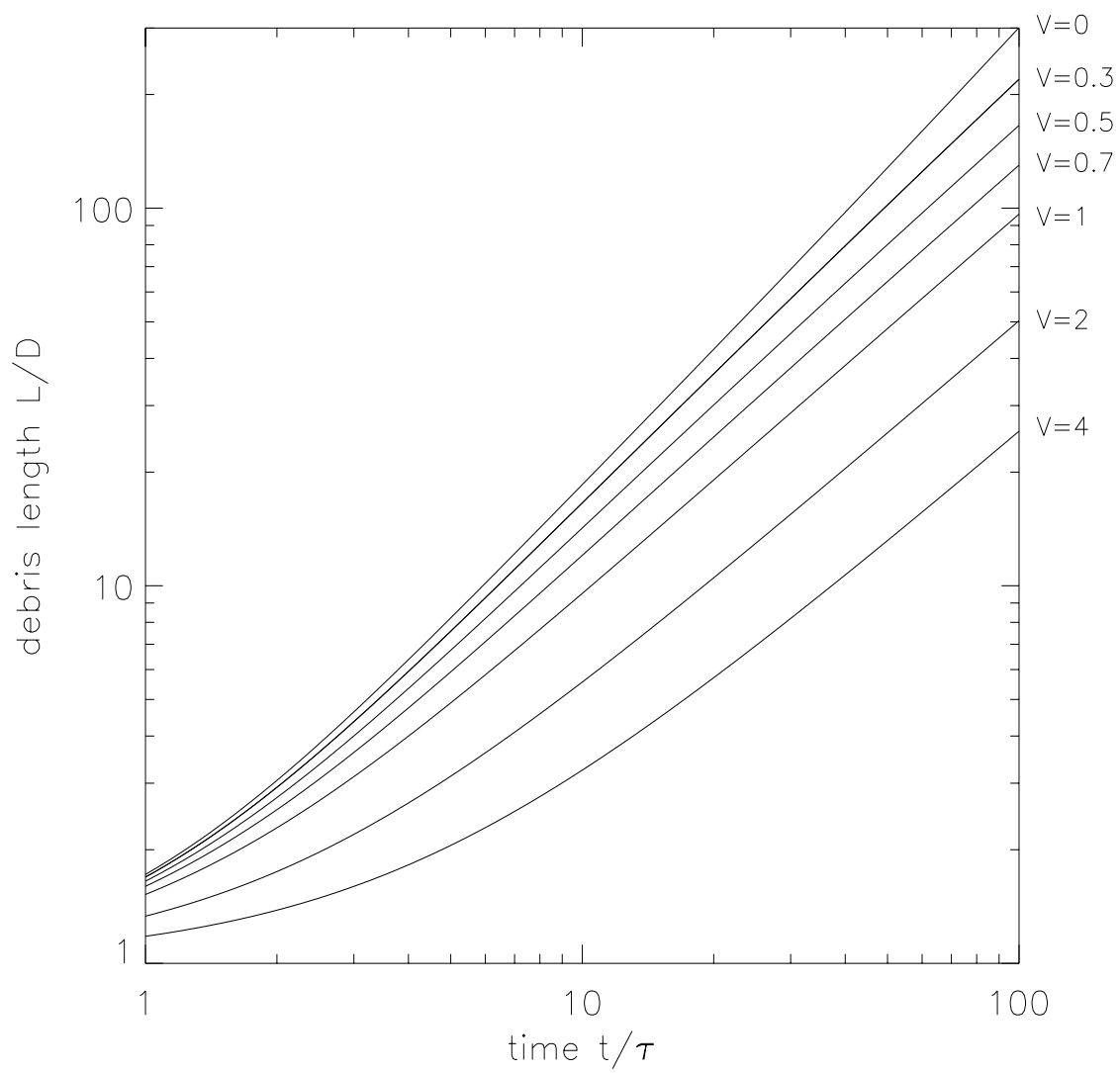


Fig. 4

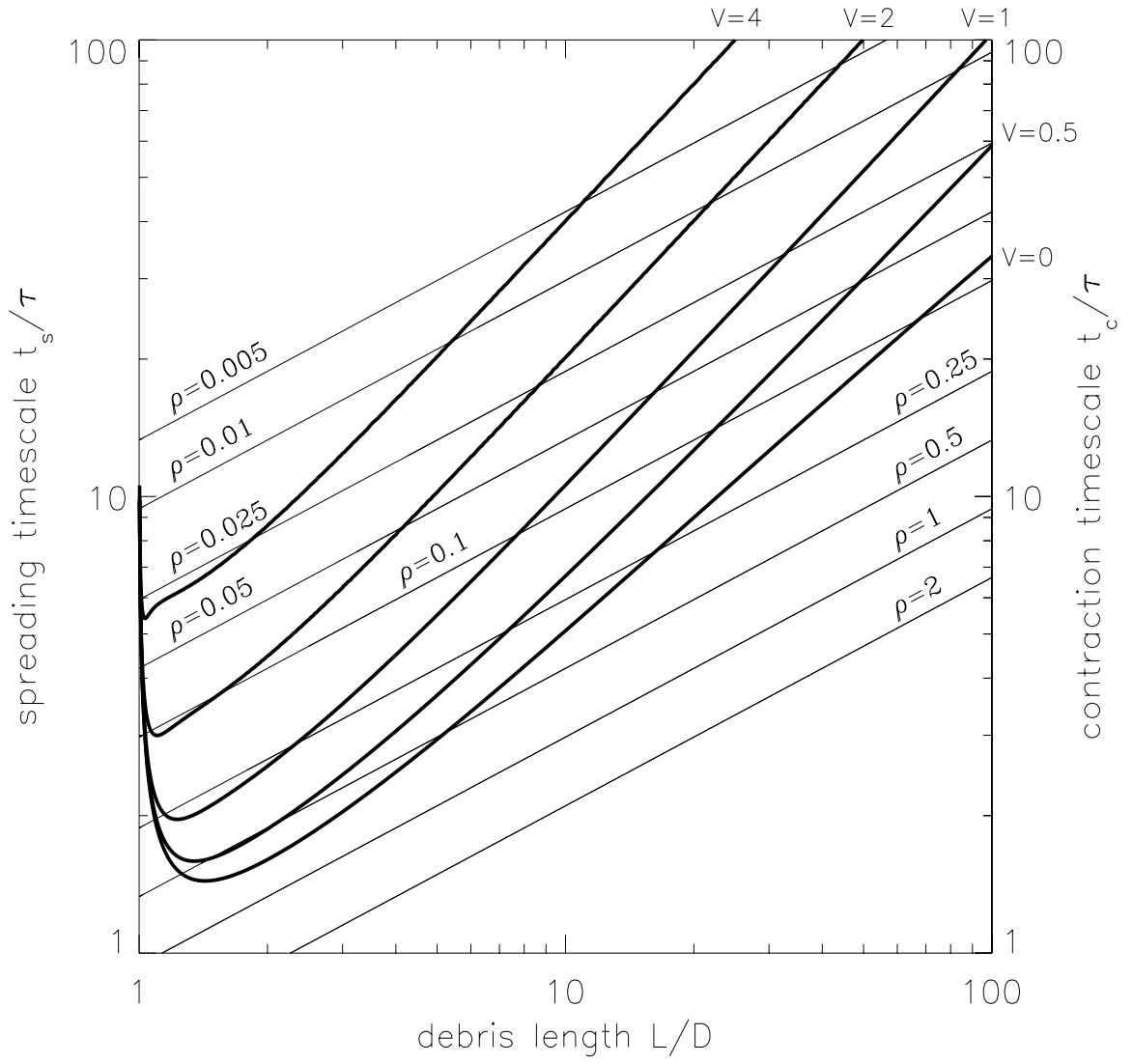


Fig. 5

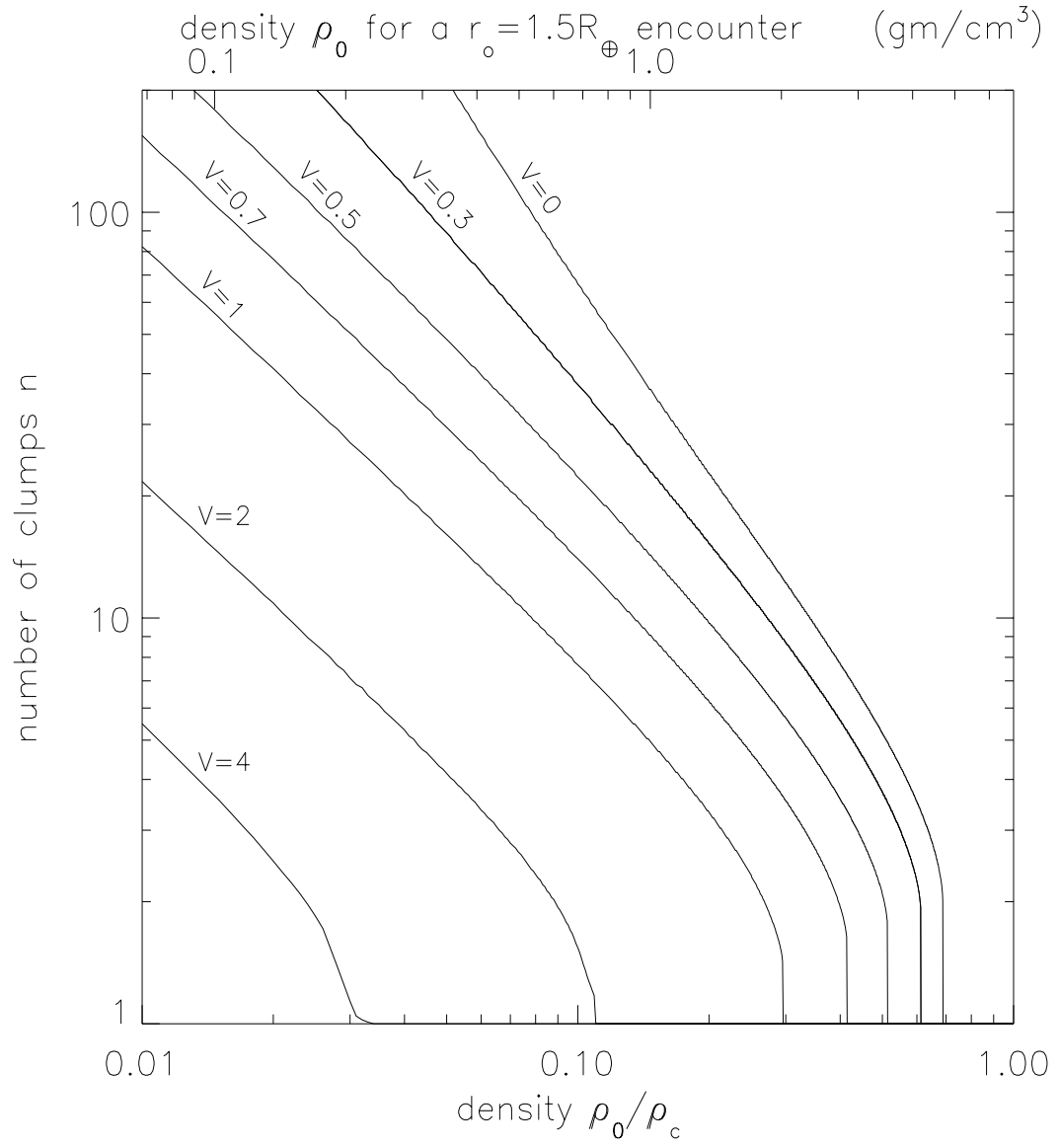


Fig. 6